The Black Hole Remnant of Black Hole-Neutron Star Coalescing Binaries

Francesco Pannarale[1]

[1]*Max-Planck-Institut für Gravitationsphysik, Albert Einstein Institut, Potsdam, Germany*

We present a model for determining the dimensionless spin parameter and mass of the black hole remnant of black hole-neutron star mergers with parallel orbital angular momentum and initial black hole spin. This approach is based on the Buonanno, Kidder, and Lehner method for binary black holes and it is successfully tested against the results of numerical-relativity simulations: the dimensionless spin parameter is predicted with absolute error $\lesssim 0.02$, whereas the relative error on the final mass is $\lesssim 2\%$, its distribution being pronouncedly peaked at 1%. Our approach and the fit to the torus remnant mass reported in [1] thus constitute an easy-to-use analytical model that accurately describes the remnant of BH-NS mergers. We investigate the space of parameters consisting of the binary mass ratio, the initial black hole spin, and the neutron star mass and equation of state. We provide indirect support to the cosmic censorship conjecture for black hole remnants of black hole-neutron star mergers. We show that the presence of a neutron star affects the quasi-normal mode frequency of the black hole remnant, thus suggesting that the ringdown epoch of the gravitational wave signal may virtually be used to (1) distinguish binary black hole from black hole-neutron star mergers and to (2) constrain the neutron star equation of state.

I. INTRODUCTION

Once a black hole-neutron star (BH-NS) binary is formed, gravitational radiation reaction gradually reduces its orbital separation until the two objects merge and leave behind a remnant consisting of a black hole and, possibly, a hot, massive accretion torus surrounding it [2]. BH-NS binaries have not been observed yet; population synthesis studies, however, suggest that the coalescence of BH-NS systems is likely to occur frequently in the Hubble volume, thus making theoretical studies on the evolution and final state of BH-NS mergers relevant [3–7]. Interest in these systems arises from the fact that they are among the most promising sources for gravitational wave (GW) detectors — such as LIGO [8], Virgo [9], KAGRA [10], and the Einstein Telescope [11] — and that they are promising candidates as progenitors of (a fraction of) short-hard gamma-ray bursts [12, 13]. Further, as NSs in these systems undergo strong tidal deformations, observing GW and/or electromagnetic signals emitted by BH-NS binaries could help shed light on the equation of state (EOS) of matter at supra-nuclear densities, which is currently unknown [14–17]. Finally, comprehending the fate of the material possibly ejected by BH-NS binaries after the NS tidal disruption is relevant in interpreting the observed abundances of the heavy elements that are formed by rapid neutron capture in r-processes [18].

To achieve a full understanding of BH-NS merger events and their physics, numerical-relativity simulations are required. These will ultimately have to include adequate and accurate treatments of General Relativity, relativistic (magneto)hydrodynamics, the microphysical EOS, NS crust physics, thermal effects, nuclear physics reactions. Numerical quasi-equilibrium studies [19–25] and dynamical simulations [17, 26–48] of mixed binary mergers made considerable progress in the last few years. Despite the fact that simulating BH-NS mergers is now possible, these simulations remain nevertheless both challenging and computationally intensive. These problems have motivated the parallel development of

pseudo-Newtonian BH-NS calculations, e.g. [49], and of analytical approaches focusing on specific physical aspects of the problem, e.g. [1, 14–16, 50–56]. Studies of these kinds benefit of their low computational costs which allow them to shed light on questions that cannot be currently addressed with numerical simulations and to provide insight on what happens when one spans the large space of parameters of BH-NS binaries. They may, in turn, aid in orienting numerical-relativity efforts by suggesting particularly interesting cases to simulate and in providing information to exploit within the simulations themselves.

In this paper we focus on predicting the final spin parameter and mass of the BH remnant of BH-NS coalescing binaries by using a semi-analytical approach. While this problem has a fairly long history in the case of coalescing binary black holes [57–77], no attempt beyond numerical-relativity simulations has yet been made to tackle it in the case BH-NS mergers. The approach we present and discuss is based on the work of Buonanno, Kidder, and Lehner (BKL) on estimating the final BH spin of a coalescing binary BH with arbitrary initial masses and spins [66]. We choose this simple, phenomenological model as a starting point because it provides good physical insight and it is straightforward to modify and extend. Our method may indeed be seen as a generalization of the BKL model to the case in which the lower mass BH is replaced with a NS. It is, however, restricted to systems in which the BH spin direction is parallel to the orbital angular momentum direction. This is due to the small number of numerical-relativity simulations available for non-aligned BH spin and orbital angular momentum configurations [43]. The closed expression we determine for the final spin parameter automatically yields an estimate of the mass of the BH remnant by means of a method similar to the starting point of Barausse, Morozova, and Rezzolla's calculations on the mass radiated by binary BHs [77], but with modifications inspired, once again, by [66]. The key equations of our approach are Eqs. (9), (11)-(12) and, despite the mathematical complexity of the mixed binary coalescence problem, our method enables

us to reproduce the results of numerical-relativity simulations with reasonable accuracy.

The paper is organized as follows. In Section II we review the BKL approach for binary BHs. In Section III we propose an extension of this method in order to predict the final spin parameter and mass of BH remnants of BH-NS mergers — Eqs. (9), (11)-(12) — and successfully test it against available numerical-relativity data. In Section IV we gather the results obtained by systematically varying the binary mass ratio, the initial BH spin parameter, and the NS mass and EOS. First, we provide indirect support to cosmic censorship conjecture and suggest particularly interesting cases to explore with numerical simulations in this context (Section IV A). Then, we show that the NS EOS may leave an imprint on the BH remnant in terms of its final spin and mass (Section IV B). This suggests the idea of inferring the presence of the NS and of constraining its EOS from the ringdown of the BH remnant. Finally, in Section V, we draw our conclusions and collect our remarks.

II. THE BKL FORMULA

The Buonanno, Kidder, and Lehner (BKL) approach to estimate the final spin of BH-BH mergers [66] starts by considering an initial reference state with two widely separated black holes approximated as two Kerr black holes having masses $\{M_1, M_2\}$ and dimensionless spin parameters[1] $\{a_1, a_2\}$. The case of the BKL approach that we will extend in order to describe BH-NS binaries is that of BH binary systems the orbits of which stay within a unique plane, referred to as the equatorial plane; in such case, the orbital angular momentum and the individual spins of the BHs are orthogonal to the equatorial plane. The spin parameter of the BH remnant a_f is obtained in terms of the initial configuration of the system by a phenomenological approach relying on the following two observations based on intuitive arguments, on post-Newtonian and perturbative calculations for the inspiral and ringdown, and on numerical simulations of the merger.

1. The system evolves quasi-adiabatically during the inspiral phase.

2. The total mass and angular momentum of the system change only by a small amount during the merger and ringdown phases.

Further, the BKL expression for a_f is derived from first principles once the following assumptions are made:

3. The mass of the system is conserved to first order, so that the final BH has a total mass $M = M_1 + M_2$.

4. The magnitude of the individual BH spins remains constant and their contribution to the final total angular momentum is determined by the their initial values.

5. The system radiates much of its angular momentum in the long inspiral stage until it reaches the innermost stable circular orbit (ISCO), when the dynamics quickly leads to the merger of the two BHs. Given that the radiation of energy and angular momentum during the merger is small with respect to the mass and angular momentum of the system, the contribution of the orbital angular momentum to the angular momentum of the BH remnant is estimated by considering the orbital angular momentum of a test-particle orbiting a Kerr BH, with spin parameter equal to that of the *final* BH, at the ISCO.

All these assumptions are combined in the following formula expressing the dimensionless spin parameter of the final BH:

$$a_f = \frac{a_1 M_1^2 + a_2 M_2^2 + l_z(\bar{r}_{ISCO,f}, a_f) M_1 M_2}{M^2}, \quad (1)$$

where $l_z(\bar{r}_{ISCO,f}, a_f)$ is the orbital angular momentum per unit mass of a test-particle orbiting the BH remnant at the ISCO, and where we introduced the notation $\bar{r} = r/M$ for the (dimensionless) Boyer-Lindquist radial coordinate.

We recall that for equatorial orbits around a Kerr BH of spin parameter a

$$l_z(\bar{r}, a) = \pm \frac{\bar{r}^2 \mp 2a\sqrt{\bar{r}} + a^2}{(\bar{r}^2 - 3\bar{r} \pm 2a\sqrt{\bar{r}})\sqrt{\bar{r}}} \quad (2)$$

and that the orbital separation at the ISCO is given by

$$\bar{r}_{ISCO} = [3Z_2 \mp \sqrt{(3 - Z_1)(3 + Z_1 + 2Z_2)}]$$
$$Z_1 = 1 + (1 - a^2)^{1/3} \left[(1 + a)^{1/3} + (1 - a)^{1/3}\right]$$
$$Z_2 = \sqrt{3a^2 + Z_1^2}, \quad (3)$$

where the upper/lower signs hold for co/counter-rotating orbits. Throughout the paper we will use the symbols $\bar{r}_{ISCO,i}$ and $\bar{r}_{ISCO,f}$ to denote $\bar{r}_{ISCO}$ calculated for the initial and the final BH spin parameter, respectively. In the following, we will also be using the energy per unit mass e of a test-particle orbiting a BH. It may be expressed as

$$e(\bar{r}, a) = \frac{\bar{r}^2 - 2\bar{r} \pm a\sqrt{\bar{r}}}{(\bar{r}^2 - 3\bar{r} \pm 2a\sqrt{\bar{r}})\sqrt{\bar{r}}} \quad (4)$$

for Kerr equatorial orbits.

III. A MODEL FOR BH-NS MERGERS

When modifying Eq. (1) in order to describe BH-NS systems, the first step is to set the initial spin angular momentum of the NS to zero since (1) this is believed to be a reliable approximation of astrophysically realistic systems [78, 79] and (2) this was done in all BH-NS merger numerical simulations so far and we use these as test cases to assess the validity of

---

[1] BKL use a's with the dimensions of a mass, while we use dimensionless a's throughout this paper.

our model. Adapting the notation in Eq. (1) to BH-NS binaries, we now have

$$a_{\rm f} = \frac{a_{\rm i} M_{\rm BH}^2 + l_z(\bar{r}_{\rm ISCO,f}, a_{\rm f}) M_{\rm BH} M_{\rm NS}}{M^2} \,. \quad (5)$$

In the case of disruptive BH-NS mergers, an accretion torus surrounding the BH remnant may be formed and one must thus drop assumption 3 of the BKL approach and adequately modify Eq. (5) to take this possibility into account. This is done by:

1. replacing the term $l_z(\bar{r}_{\rm ISCO,f}, a_{\rm f}) M_{\rm BH} M_{\rm NS}$ in the numerator with $l_z(\bar{r}_{\rm ISCO,f}, a_{\rm f}) M_{\rm BH}(M_{\rm NS} - M_{\rm b,torus})$ and by

2. replacing M with $M - e(\bar{r}_{\rm ISCO,f}, a_{\rm f}) M_{\rm b,torus}$ in the denominator,

where $M_{\rm b,torus}$ is the baryonic mass of the torus remnant. The former/latter replacement expresses the lack of angular momentum/mass accretion onto the BH, due the formation of the torus. In the case of no torus formation, $M_{\rm b,torus} = 0$ and full accretion of both mass and angular momentum onto the BH is achieved. Our formula now reads

$$a_{\rm f} = \frac{a_{\rm i} M_{\rm BH}^2 + l_z(\bar{r}_{\rm ISCO,f}, a_{\rm f}) M_{\rm BH}(M_{\rm NS} - M_{\rm b,torus})}{[M - e(\bar{r}_{\rm ISCO,f}, a_{\rm f}) M_{\rm b,torus}]^2} \,, \quad (6)$$

where we once more emphasize that e and l_z are calculated for the ISCO and spin of the *final* BH.

A final element to take into account is that GW emission during the inspiral will further reduce the energy M that the system has at infinite orbital separation. This was not considered in the BKL model (see assumption 3 in the previous section), but we wish to include it in our extension of their formulation. It affects the denominator of Eq. (6) and may be taken into account at first order in the symmetric mass ratio $\nu = M_{\rm BH} M_{\rm NS}/(M_{\rm BH} + M_{\rm NS})^2$ by subtracting to M the additional term, e.g. [77],

$$E_{\rm rad} = M[1 - e(\bar{r}_{\rm ISCO,i}, a_{\rm i})]\nu \,, \quad (7)$$

so that

$$a_{\rm f} = \frac{a_{\rm i} M_{\rm BH}^2 + l_z(\bar{r}_{\rm ISCO,f}, a_{\rm f}) M_{\rm BH}(M_{\rm NS} - M_{\rm b,torus})}{[M\{1 - [1 - e(\bar{r}_{\rm ISCO,i}, a_{\rm i})]\nu\} - e(\bar{r}_{\rm ISCO,f}, a_{\rm f}) M_{\rm b,torus}]^2} \,. \quad (8)$$

This final, closed expression for the final spin parameter $a_{\rm f}$ may be solved with root-finding techniques to numerically determine the spin parameter of the BH remnant of BH-NS mergers and its denominator naturally provides a prediction for the final mass of the remnant itself. In other words, once $a_{\rm f}$ is calculated, the mass of the BH remnant $M_{\rm f}$ automatically follows as

$$M_{\rm f} = M\{1 - [1 - e(\bar{r}_{\rm ISCO,i}, a_{\rm i})]\nu\} - e(\bar{r}_{\rm ISCO,f}, a_{\rm f}) M_{\rm b,torus} \,. \quad (9)$$

Notice that, in principle, Eq. (8) may be generalized to account for additional energy losses and for non ideal angular momentum accretion. In the former case, it is sufficient to subtract extra terms on the right hand side of Eq. (9) and, hence, in the denominator of Eq. (8). Non ideal angular momentum accretion, which is particularly relevant for disruptive BH-NS mergers, could instead be modelled by inserting an angular momentum accretion efficiency factor in front of the l_z appearing in Eq. (8). For the time being, we keep Eq. (8) as it is, knowing that it may be improved as the nuances in the physics of BH-NS mergers become clearer.

In Tables I and II we compare the predictions of Eq. (8) and Eq. (1) to the results obtained within full General Relativity in [38, 43–46, 48], which, along with [17, 47], represent the state of the art of numerical-relativity simulations of BH-NS mergers. The BKL predictions are reported in column seven and denoted with $a_{\rm f}^{\rm BKL}$, whereas the outcomes of Eq. (8) are given in column eight and denoted with $a_{\rm f,1}$ since we will shortly improve our model further. Each row of the tables refers to a specific BH-NS binary coalescence and its columns provide a dummy index which numbers the test cases, the reference in which the numerical-relativity simulation for that binary was presented, information about the NS EOS, the NS compactness $C = M_{\rm NS}/R_{\rm NS}$, the binary mass ratio $Q = M_{\rm BH}/M_{\rm NS}$, the initial BH spin parameter $a_{\rm i}$, the numerical-relativity result for the final BH spin parameter $a_{\rm f}^{\rm NR}$, the final BH spin parameter $a_{\rm f}^{\rm BKL}$ predicted by the BKL formula in Eq. (1), the final BH spin parameter $a_{\rm f,1}$ yielded by Eq. (8), and the final BH spin parameter $a_{\rm f}$ predicted by Eq. (11), which we discuss later. As far as the NS EOS is concerned, the first 19 comparisons reported in Table I refer to binaries in which the non-thermal behaviour of the NS matter[2] is governed, at microphysical level, by a polytropic EOS with polytropic exponent $\Gamma = 2$. In the last 18 simulations reported in Table I and in all the ones reported in Table II, on the other hand, a two-piecewise polytropic EOS was used and the notation in the tables follows the one used in [41] and [44]: the first half of the label indicates the stiffness of the EOS, 2H being the stiffest, whereas the second half refers to the NS ADM mass at isolation (e.g. 135 stands for $1.35 M_\odot$). In this first round of tests, we used the values of $M_{\rm b,torus}$ found with the numerical-relativity simulations and reported in the papers. To make the whole model numerical-relativity-independent and of quick use, we shall later adopt the method recently reported in [1] for determining $M_{\rm b,torus}$ and we will show that the use of such method for estimating $M_{\rm b,torus}$ does not spoil the agreement between the predictions of our model and the numerical-relativity data for the final BH spin parameter. It is evident that the difference between $a_{\rm f,1}$ and $a_{\rm f}^{\rm NR}$ increases as the mass ratio Q of the system decreases, or, equivalently, as the symmetric mass ratio ν increases. Given that the final spin parameter results obtained with numerical-relativity simulations have an absolute error $\Delta a_{\rm f}^{\rm NR}$ of 0.01 [39] and that the error of the BKL approach was evaluated to be $\lesssim 0.02$ in [75], we conclude that the method established by Eq. (8) works well for BH-NS systems with symmetric mass ratios

_____

[2] Here and in [1, 56] thermal contributions are neglected. These are more relevant, in the merger and post-merger dynamics, if the NS is tidally disrupted.

up to $\nu = 0.1875$, i.e. for $Q \geq 3$, whereas it almost systematically exceeds the 0.03 threshold of marginal agreement for binaries in which $Q = 2$. We must, thus, improve Eq. (8) to

handle BH-NS systems with $\nu > 0.1875$.

As ν increases, the method fails for two reasons. Firstly, the fifth assumption in Section II breaks down as $\nu \to 0.25$ (or $Q \to 1$): this is intrinsic to the BKL method which inspired Eq. (8). Secondly, and generally speaking, in systems with such low mass BHs the tidal fields tend to tear apart the NS completely, as opposed to in binaries with higher mass BHs, in which the outer layers of the NS are mainly stripped off. In the former scenario, the binding energy of the star is liberated and the NS matter accretes onto the BH as a collection of particles with total rest mass $M_{b,NS} - M_{b,torus}$, where $M_{b,NS}$ is the total rest mass of the NS, whereas in the latter scenario the NS

TABLE I. Tests against numerical-relativity results. Each row is a test-case numbered by the index in the first column. The remaining columns provide the reference in which the numerical-relativity simulation for the binary was presented, information about the NS EOS, the NS compactness C, the binary mass ratio Q, the initial BH spin parameter a_i, and the final BH spin parameter given by the numerical-relativity simulation, a_f^{NR}, by the BKL approach, a_f^{BKL}, by Eq. (8), $a_{f,1}$, and by the final formulation of our model given in Eqs. (11) and (12), a_f. The NSs in the initial data of all simulations are spinless.

	Ref.	EOS	C	Q	a_i	a_f^{NR}	a_f^{BKL}	$a_{f,1}$	a_f
1	[38]	$\Gamma = 2$	0.145	3	-0.5	0.33	0.31	0.31	0.31
2	[38]	$\Gamma = 2$	0.145	3	0.75	0.88	0.85	0.86	0.86
3	[38]	$\Gamma = 2$	0.145	3	0	0.56	0.54	0.53	0.53
4	[38]	$\Gamma = 2$	0.145	5	0	0.42	0.42	0.42	0.42
5	[48]	$\Gamma = 2$	0.145	2	0	0.68	0.61	0.61	0.64
6	[48]	$\Gamma = 2$	0.145	3	0	0.56	0.54	0.53	0.53
7	[48]	$\Gamma = 2$	0.145	4	0	0.48	0.47	0.47	0.47
8	[48]	$\Gamma = 2$	0.145	5	0	0.42	0.42	0.42	0.42
9	[48]	$\Gamma = 2$	0.160	2	0	0.68	0.61	0.62	0.65
10	[48]	$\Gamma = 2$	0.160	3	0	0.55	0.54	0.54	0.54
11	[48]	$\Gamma = 2$	0.178	2	0	0.67	0.61	0.62	0.66
12	[48]	$\Gamma = 2$	0.178	3	0	0.55	0.54	0.54	0.54
13	[43]	$\Gamma = 2$	0.144	3	0	0.56	0.54	0.53	0.53
14	[43]	$\Gamma = 2$	0.144	3	0.5	0.77	0.75	0.75	0.75
15	[43]	$\Gamma = 2$	0.144	3	0.9	0.93	0.90	0.93	0.93
16	[46]	$\Gamma = 2$	0.144	7	0.5	0.67	0.67	0.68	0.68
17	[46]	$\Gamma = 2$	0.144	7	0.7	0.80	0.80	0.81	0.81
18	[46]	$\Gamma = 2$	0.144	7	0.9	0.92	0.91	0.93	0.93
19	[46]	$\Gamma = 2$	0.144	5	0.5	0.71	0.71	0.71	0.71
20	[45]	2H-135	0.131	2	0	0.64	0.61	0.59	0.63
21	[45]	H-135	0.162	2	0	0.67	0.61	0.61	0.66
22	[45]	HB-135	0.172	2	0	0.67	0.61	0.62	0.66
23	[45]	HBs-135	0.172	2	0	0.67	0.61	0.62	0.66
24	[45]	HBss-135	0.174	2	0	0.67	0.61	0.62	0.66
25	[45]	B-135	0.182	2	0	0.67	0.61	0.62	0.67
26	[45]	Bs-135	0.185	2	0	0.66	0.61	0.62	0.67
27	[45]	Bss-135	0.194	2	0	0.65	0.61	0.62	0.67
28	[45]	2H-135	0.131	3	0	0.52	0.54	0.51	0.51
29	[45]	H-135	0.162	3	0	0.56	0.54	0.54	0.54
30	[45]	HB-135	0.172	3	0	0.56	0.54	0.54	0.54
31	[45]	B-135	0.182	3	0	0.55	0.54	0.54	0.54
32	[45]	2H-12	0.118	2	0	0.62	0.61	0.58	0.62
33	[45]	H-12	0.145	2	0	0.66	0.61	0.60	0.64
34	[45]	HB-12	0.153	2	0	0.66	0.61	0.61	0.65
35	[45]	B-12	0.161	2	0	0.67	0.61	0.61	0.66
36	[45]	HB-12	0.153	3	0	0.55	0.54	0.54	0.54
37	[45]	B-12	0.161	3	0	0.56	0.54	0.54	0.54

TABLE II. Same as Table I.

	Ref.	EOS	C	Q	a_i	a_f^{NR}	a_f^{BKL}	$a_{f,1}$	a_f
38	[44]	2H-135	0.131	2	0.75	0.87	0.84	0.86	0.89
39	[44]	1.5H-135	0.146	2	0.75	0.89	0.84	0.86	0.89
40	[44]	H-135	0.162	2	0.75	0.91	0.84	0.86	0.90
41	[44]	HB-135	0.172	2	0.75	0.91	0.84	0.86	0.90
42	[44]	B-135	0.182	2	0.75	0.91	0.84	0.86	0.90
43	[44]	2H-135	0.131	2	0.5	0.81	0.77	0.77	0.80
44	[44]	1.5H-135	0.146	2	0.5	0.82	0.77	0.77	0.81
45	[44]	H-135	0.162	2	0.5	0.82	0.77	0.78	0.82
46	[44]	HB-135	0.172	2	0.5	0.83	0.77	0.78	0.82
47	[44]	B-135	0.182	2	0.5	0.83	0.77	0.78	0.82
48	[44]	2H-135	0.131	2	-0.5	0.48	0.44	0.42	0.46
49	[44]	H-135	0.162	2	-0.5	0.51	0.44	0.45	0.50
50	[44]	HB-135	0.172	2	-0.5	0.50	0.44	0.45	0.50
51	[44]	B-135	0.182	2	-0.5	0.49	0.44	0.45	0.51
52	[44]	2H-135	0.131	3	0.75	0.86	0.85	0.86	0.86
53	[44]	1.5H-135	0.146	3	0.75	0.86	0.85	0.86	0.86
54	[44]	H-135	0.162	3	0.75	0.85	0.85	0.86	0.86
55	[44]	HB-135	0.172	3	0.75	0.87	0.85	0.86	0.86
56	[44]	B-135	0.182	3	0.75	0.86	0.85	0.87	0.87
57	[44]	2H-135	0.131	3	0.5	0.74	0.75	0.74	0.74
58	[44]	1.5H-135	0.146	3	0.5	0.75	0.75	0.75	0.75
59	[44]	H-135	0.162	3	0.5	0.76	0.75	0.75	0.75
60	[44]	HB-135	0.172	3	0.5	0.77	0.75	0.76	0.76
61	[44]	B-135	0.182	3	0.5	0.77	0.75	0.76	0.76
62	[44]	HB-135	0.172	3	-0.5	0.32	0.31	0.31	0.31
63	[44]	2H-135	0.131	4	0.75	0.84	0.84	0.85	0.85
64	[44]	H-135	0.162	4	0.75	0.84	0.84	0.86	0.86
65	[44]	HB-135	0.172	4	0.75	0.85	0.84	0.86	0.86
66	[44]	B-135	0.182	4	0.75	0.85	0.84	0.86	0.86
67	[44]	2H-135	0.131	4	0.5	0.70	0.73	0.71	0.71
68	[44]	H-135	0.162	4	0.5	0.73	0.73	0.73	0.73
69	[44]	HB-135	0.172	4	0.5	0.74	0.73	0.74	0.74
70	[44]	B-135	0.182	4	0.5	0.74	0.73	0.74	0.74
71	[44]	2H-135	0.131	5	0.75	0.82	0.84	0.84	0.84
72	[44]	H-135	0.162	5	0.75	0.84	0.84	0.85	0.85
73	[44]	HB-135	0.172	5	0.75	0.84	0.84	0.85	0.85
74	[44]	B-135	0.182	5	0.75	0.85	0.84	0.86	0.86

core plunges into the BH without undergoing complete tidal disruption. We will make the simplifying assumption that in systems with $\nu = 2/9$ ($Q = 2$) the NS undergoes complete tidal disruption, while it does not in systems with $\nu \leq 0.1875$ ($Q \geq 3$). As mentioned, when complete tidal disruption is achieved, the NS should not be treated as a body with mass M_{NS}, but as a set of particles with total rest mass $M_{\text{b,NS}}$, a fraction of which accretes onto the BH, this fraction having

a total mass $M_{\text{b,NS}} - M_{\text{b,torus}}$. We thus propose to describe $Q = 2$ systems, in which tidal disruption is pivotal, with

$$a_{\text{f}} = \frac{aM_{\text{BH}}^2 + l_z(\bar{r}_{\text{ISCO,f}}, a_{\text{f}})M_{\text{BH}}(M_{\text{b,NS}} - M_{\text{b,torus}})}{[M\{1 - [1 - e(\bar{r}_{\text{ISCO,i}}, a_{\text{i}})]\nu\} - e(\bar{r}_{\text{ISCO,f}}, a_{\text{f}})M_{\text{b,torus}}]^2} \tag{10}$$

instead of with Eq. (8) and to combine the two description by writing

$$a_{\text{f}} = \frac{aM_{\text{BH}}^2 + l_z(\bar{r}_{\text{ISCO,f}}, a_{\text{f}})M_{\text{BH}}\{f(\nu)M_{\text{b,NS}} + [1 - f(\nu)]M_{\text{NS}} - M_{\text{b,torus}}\}}{[M\{1 - [1 - e(\bar{r}_{\text{ISCO,i}}, a_{\text{i}})]\nu\} - e(\bar{r}_{\text{ISCO,f}}, a_{\text{f}})M_{\text{b,torus}}]^2} \tag{11}$$

where $f(\nu)$ governs the transition between the two regimes. This function is currently poorly constrained since state-of-the-art BH-NS simulations with $2 < Q < 3$ are not are available in the literature and we have a lot of freedom in choosing it. To fix $f(\nu)$, we must impose that $f(\nu \geq 2/9) = 1$ and that $f(\nu \leq 0.1875) = 0$. Additionally, it is physically reasonable to require the function to be monotonic and therefore that

$$\frac{df}{d\nu} \geq 0 \qquad 0 \leq \nu \leq 0.25 \, .$$

We shall also require it to be C^∞ and to be as simple as possible. These elements do not determine $f(\nu)$ uniquely, of course. All in all, we set

$$f(\nu) = \begin{cases} 0 & \nu \leq 0.1875 \\ \frac{1}{2}\left[1 - \cos\left(\frac{\pi(\nu - 0.1875)}{2/9 - 0.1875}\right)\right] & 0.1875 < \nu < 2/9 \\ 1 & \nu \geq 2/9 \end{cases} \tag{12}$$

in a Hann window inspired fashion. Notice that, in the limit of large BH masses, a BH-NS systems behaves as a BH binary

system with the same physical parameters, so that one cannot simply drop the NS gravitational mass M_{NS} in favour of its baryonic mass $M_{\text{b,NS}}$ in Eq. (8). Moreover, from a merely quantitative point of view, a model with this oversimplification performs worse when tested against numerical-relativity results.

We now compare the predictions of Eqs. (11)-(12) to the results obtained within full General Relativity. As anticipated, this is done in the last column of Tables I and II. By inspecting the last columns in the tables, it is evident that this strategy considerably improves the outcome of Eq. (8) for $Q = 2$ systems and that it overall improves the estimates obtained by simply applying the BKL method to mixed binary mergers.

Figure 1 shows the absolute value of the difference $a_{\text{f}} - a_{\text{f}}^{\text{NR}}$ versus the dummy index running over the 74 rows of Tables I and II. The graph shows that $\max|a_{\text{f}} - a_{\text{f}}^{\text{NR}}| = 0.04$ and that this value is reached only in one case out of 74 total ones. This corresponds to the $\{C = 0.145, Q = 2, a_{\text{i}} = 0\}$ simulation of [39, 48]. An absolute error $|a_{\text{f}} - a_{\text{f}}^{\text{NR}}| = 0.03$ is obtained in four cases, namely the $\{C = 0.145, Q = 3, a_{\text{i}} = 0\}$ case of [38], the $\{C = 0.145, Q = 3, a_{\text{i}} = 0\}$ and $\{C = 0.160, Q = 2, a_{\text{i}} = 0\}$ binaries of [39, 48], and the $\{C = 0.144, Q = 4, a_{\text{i}} = 0\}$ test-case of [43] (i.e. test-cases
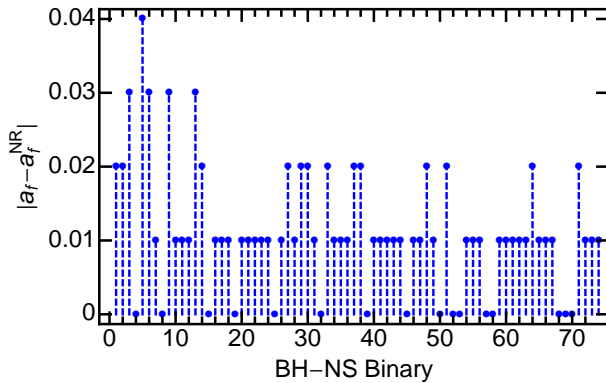

FIG. 1. $|a_{\text{f}} - a_{\text{f}}^{\text{NR}}|$ is shown for all entries in Tables I and II. The horizontal axis is the dummy that runs through both tables.
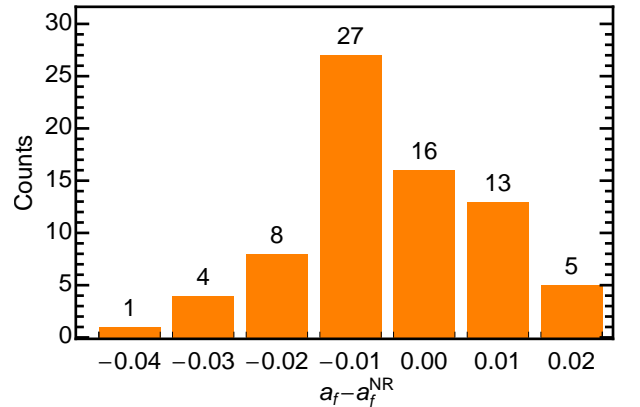

FIG. 2. $a_{\text{f}} - a_{\text{f}}^{\text{NR}}$ distribution for all entries in Tables I and II.

3, 6, 9, and 13). Notice that two of these binaries coincide. We also notice that in four of these problematic cases $C \sim 0.145$ and this may be a sign that our model breaks down for low NS compactness.

In Figure 2, we show the distribution of the differences between our predictions and the numerical relativity results for the spin parameter of the BH remnant of the BH-NS mergers of Tables I and II. As is evident, $a_\mathrm{f} - a_\mathrm{f}^\mathrm{NR} = -0.01$ is the difference getting most hits, with 27 test-cases out of 74, and about a fifth of the final spins are predicted exactly. We also notice that the distribution is slightly skewed towards negative values of $a_\mathrm{f} - a_\mathrm{f}^\mathrm{NR}$ and that the sum of all the differences $a_\mathrm{f} - a_\mathrm{f}^\mathrm{NR}$ yields -0.35, so that the average error $\sum_{n=1}^{74}(a_\mathrm{f} - a_\mathrm{f}^\mathrm{NR})_n/74 = 0.00$ is found when rounding up to the second significant figure[3]. In Figure 3, we consider the distribution of the absolute difference $|a_\mathrm{f} - a_\mathrm{f}^\mathrm{NR}|$, showing that it rapidly drops after 0.02. Given that the error on the a_f^NR's is $\Delta a_\mathrm{f}^\mathrm{NR} = 0.01$, 55 numerical-relativity results out of 74, i.e. more than 2/3 of the cases, are reproduced within the numerical-relativity error. If we take the error $\Delta a_\mathrm{f} = 0.01$ on our results, which is reasonable since (1) our model is built against the numerical-relativity data and (2) it is based on the BKL approach, for which $\Delta a_\mathrm{f}^\mathrm{BKL} \lesssim 0.02$ [75], we see that our results are compatible with the numerical-relativity ones in 69 test-cases out of 74, i.e. about 93%. A more conservative choice would be to consider $\Delta a_\mathrm{f} = 0.02$ (which is still in agreement with $\Delta a_\mathrm{f}^\mathrm{BKL}$) and *all but one* results would be completely compatible.

We notice that the value $\Delta a_\mathrm{f} = 0.01$ for the error on our predictions is also supported by the fact that $\sum_{n=1}^{74}|a_\mathrm{f} - a_\mathrm{f}^\mathrm{NR}|_n/74 = 0.01$. The same result is obtained if the average is restricted to a specific value of Q or a_i, out of the ones available in Tables I and II. These results are collected in the second column of Table III, along with the average $a_\mathrm{f} - a_\mathrm{f}^\mathrm{NR}$ marginalized to a given mass ratio or initial BH spin parameter value, which is instead reported in column four.
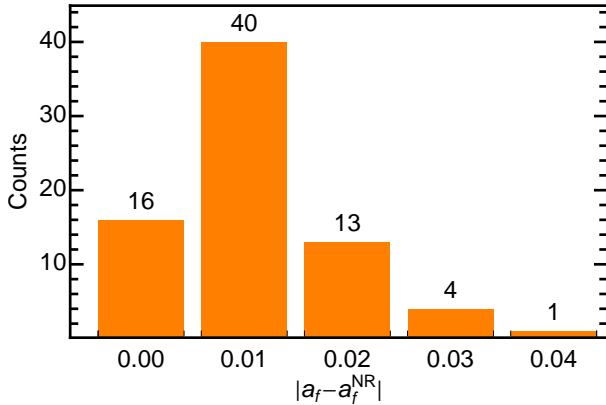
TABLE III. Average $|a_\mathrm{f} - a_\mathrm{f}^\mathrm{NR}|$ and $a_\mathrm{f} - a_\mathrm{f}^\mathrm{NR}$ for a given physical parameter, indicated in the first column. The second and fourth columns refer to predictions for a_f obtained by substituting for $M_\mathrm{b,torus}$ in Eq. (11) the results found in the numerical-relativity simulations reported in [38, 41, 43, 45, 46, 48], whereas the third and fifth columns refer to predictions for a_f obtained by using the model described in [1] to calculate the $M_\mathrm{b,torus}$'s.

Fix parameter	$\langle |a_\mathrm{f} - a_\mathrm{f}^\mathrm{NR}| \rangle$		$\langle a_\mathrm{f} - a_\mathrm{f}^\mathrm{NR} \rangle$	
$Q = 2$	0.01	0.01	-0.01	0.00
$Q = 3$	0.01	0.01	-0.01	-0.01
$Q = 4$	0.01	0.01	0.01	0.00
$Q = 5$	0.01	0.01	0.01	0.00
$Q = 7$	0.01	0.01	0.01	0.01
$a_\mathrm{i} = -0.5$	0.01	0.01	-0.01	-0.01
$a_\mathrm{i} = 0$	0.01	0.02	-0.01	-0.01
$a_\mathrm{i} = 0.5$	0.01	0.01	0.00	0.00
$a_\mathrm{i} = 0.7$	0.01	0.01	0.01	0.01
$a_\mathrm{i} = 0.75$	0.01	0.01	0.00	0.00
$a_\mathrm{i} = 0.9$	0.01	0.01	0.01	0.01

Thus far, when comparing the predictions of Eqs. (11)-(12) to the BH-NS merger results available in the literature, we used, case per case, the numerical-relativity prediction for $M_\mathrm{b,torus}$. This allowed us to test and validate Eqs. (11)-(12). If we wish to apply such method to a large number and variety of BH-NS binaries, we must consider another way of obtaining $M_\mathrm{b,torus}$. As mentioned previously, we choose to use the simple two-parameter model, fitted to existing numerical results, recently reported by Foucart in [1]. This allows one to estimate $M_\mathrm{b,torus}$ for a given binary mass ratio, initial BH spin parameter, and NS compactness. In Figure 4 we show the absolute values of the difference $a_\mathrm{f} - a_\mathrm{f}^\mathrm{NR}$ obtained when using the approach of [1] to calculate $M_\mathrm{b,torus}$; this figure must be compared to Figure 1. We find that the problematic test-cases, i.e. ones with $|a_\mathrm{f} - a_\mathrm{f}^\mathrm{NR}| > 0.02$, are the same ones encountered previously, that is, cases 3, 5, 6, 9, and 13, and that this

FIG. 3. $|a_\mathrm{f} - a_\mathrm{f}^\mathrm{NR}|$ distribution for all entries in Tables I and II.
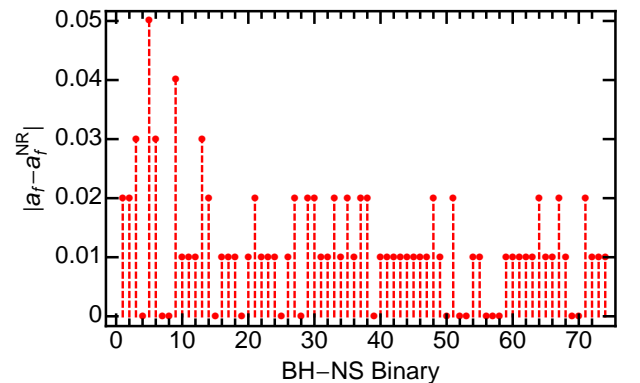
FIG. 4. Same as Figure 1, but using the predictions of [1] for $M_\mathrm{b,torus}$ in Eq. (11).

---

[3] This rounding up is justified by the fact that numerical-relativity results for the final spin parameter have an error $\Delta a_\mathrm{f}^\mathrm{NR} \sim 0.01$.

time $\max |a_{\rm f} - a_{\rm f}^{\rm NR}| = 0.05$, which occurs once.

As far as the distribution of the differences $a_{\rm f} - a_{\rm f}^{\rm NR}$ is concerned, it is again slightly skewed towards negative values: the sum over all differences $a_{\rm f} - a_{\rm f}^{\rm NR}$ yields -0.38 (as opposed to -0.35). The averages $\sum_{n=1}^{74}(a_{\rm f} - a_{\rm f}^{\rm NR})_n/74$ and $\sum_{n=1}^{74}|a_{\rm f} - a_{\rm f}^{\rm NR}|_n/74$ rounded up to the second significant figure are -0.01 and 0.01, respectively. The average differences $a_{\rm f} - a_{\rm f}^{\rm NR}$ and $|a_{\rm f} - a_{\rm f}^{\rm NR}|$ for a given binary mass ratio or initial BH spin parameter are reported in the third and fifth column of Table III, respectively. Their values are well behaved, in that they fall in the interval $[-0.01, 0.01]$, with the exception of the average $|a_{\rm f} - a_{\rm f}^{\rm NR}|$ restricted to the test-cases with $a_{\rm i} = 0$, which yields 0.02 when using the fit of [1]. The $|a_{\rm f} - a_{\rm f}^{\rm NR}|$ distribution obtained combining Eqs. (11)-(12) with the model of [1] is shown in Figure 5 and should be compared to the one in Figure 3. The distribution is again peaked around 0.01. Recalling that $\Delta a_{\rm f}^{\rm NR} = 0.01$, an agreement within the numerical-relativity error is found in 52 (as opposed to 55) cases out of 74, whereas considering $\Delta a_{\rm f} = 0.01$, one may once again state that 69 predictions out of 74 are compatible with the numerical-relativity results.

In conclusion, the tests and analysis performed for the final spin parameter $a_{\rm f}$ show that the model formulated in Eqs. (11)-(12) is robust. The error $\Delta a_{\rm f}$ on $a_{\rm f}$ that we obtain from our tests is $\Delta a_{\rm f} \lesssim 0.02$. This is compatible with the error $\Delta a_{\rm f}^{\rm NR} = 0.01$ on numerical-relativity results, against which our model is built, and with the error of the BKL model, which inspired this work. We further note that it is compatible with $\sim 1\%$ variations of the term $a_{\rm i}M_{\rm BH}^2$ appearing in Eq. (11). If we interpret this artificial $\sim 1\%$ variation as a representation of possible "glitches" in the transition from the quasi-equilibrium initial data to the dynamical evolution of the Einstein equations in a numerical simulation, we see that we are indeed "inheriting" a ~ 0.01 contribution to $\Delta a_{\rm f}$ in building our model against numerical-relativity results and that this contribution is at least comparable to the ones introduced by all other approximations behind Eqs. (11)-(12). All these conclusions remain valid even when combining Eqs. (11)-(12) with the method of [1] to calculate $M_{\rm b,torus}$.
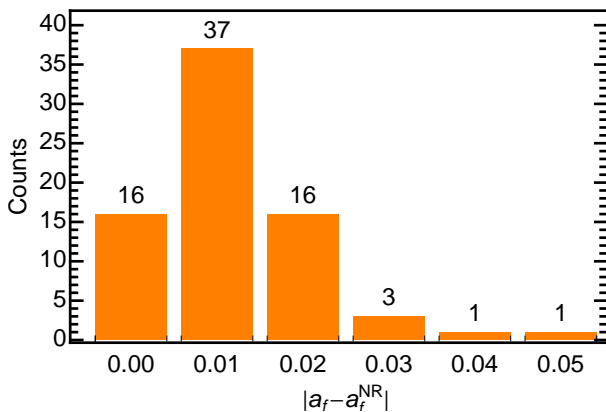

FIG. 5. $|a_{\rm f} - a_{\rm f}^{\rm NR}|$ distribution obtained when using the predictions of [1] for $M_{\rm b,torus}$ in Eq. (11).

It is striking that our simple model to determine $a_{\rm f}$ paired with [1] obtains such an excellent agreement with the fully general-relativistic numerical simulations of BH-NS mergers. One must always bear in mind, however, that there still are large, unexplored portions of the parameter space and that this prevents us from thoroughly testing our approach to determine $a_{\rm f}$.

A. Testing the Final Mass Predictions

So far, we tested only one of the two predictions that our model enables us to make. In this section we separately test the predictions for the mass $M_{\rm f}$ of the BH remnant, stemming from Eq. (9). According to the "no-hair" theorem of General Relativity, the final spin parameter and mass of an electrically neutral BH are the only two quantities characterizing the BH itself. A model capable of accurately predicting both $a_{\rm f}$ and $M_{\rm f}$ would therefore fully describe the BH remnant.

The numerical simulations of BH-NS mergers performed by the Kyoto-Tokyo group reported in [44, 45, 48] allow us to test the outcome of Eq. (9) and to establish the error associated with it. In Tables IV and V, we collect the numerical relativity data for the mass of the BH remnant and compare it to our predictions. The first six columns of the tables follow Tables I and II, including the numbering of the simulations appearing in column one. The seventh and eighth columns provide the relative error on the remnant masses obtained when comparing the predictions of Eq. (9) to the numerical-relativity results. Following [44, 45, 48], two forms of the remnant mass are considered: the gravitational mass, $M_{\rm f}$, and the irreducible mass

$$M_{\rm irr,f} = M_{\rm f}\sqrt{\frac{1 + \sqrt{1 - a_{\rm f}^2}}{2}}. \tag{13}$$

Both $M_{\rm f}$ and $M_{\rm irr,f}$ are divided by the sum M of the initial gravitational masses $M_{\rm BH}$ and $M_{\rm NS}$. In the remaining columns of the table, we give the relative error on the $l = 2$, $m = 2$, $n = 0$ quasi-normal mode (QNM) frequency, $f_{220}^{\rm QNM}$, and damping time, $\tau_{220}^{\rm QNM}$, of the BH remnant [80]. Both $a_{\rm f}$ and $M_{\rm f}$ must be used to calculate $f_{220}^{\rm QNM}$ and $\tau_{220}^{\rm QNM}$, so that $\epsilon(f_{220}^{\rm QNM})$ and $\epsilon(\tau_{220}^{\rm QNM})$ give us a sense of how our errors on the final BH spin parameter and mass propagate. The terms of comparison for the QNM frequencies and damping times are obtained by using the final mass and spin parameter values given in [44, 45, 48] and plugging them in the formulas of [80].

A maximum relative error of 1% and 2% is found for $\overline{M}_{\rm f} = M_{\rm f}/M$ and $\overline{M}_{\rm irr,f} = M_{\rm irr,f}/M$, respectively, with the 2% occurring only once. The errors on $f_{220}^{\rm QNM}$ and $\tau_{220}^{\rm QNM}$, on the other hand, are 4% at the most. It is noteworthy that the second contribution in Eq. (9), i.e. the energy loss due to GW emission, is crucial in obtaining such accurate results: if we do not include it, the maximum error on $\tau_{220}^{\rm QNM}$, for example, is 11%.

If we use input from the model of [1] and repeat these tests on $\overline{M}_{\rm f}$, $\overline{M}_{\rm irr,f}$, $f_{220}^{\rm QNM}$, and $\tau_{220}^{\rm QNM}$, the maximum errors

we obtain are 2%, 3%, 5%, and 4%, respectively. The panels of Figure 6 show the distributions of the relative errors $\epsilon(\overline{M}_{\mathrm{f}})$, $\epsilon(\overline{M}_{\mathrm{irr,f}})$, $\epsilon(f_{220}^{\mathrm{QNM}})$, and $\epsilon(\tau_{220}^{\mathrm{QNM}})$ obtained when using Eqs. (9), (11)-(12) in combination with [1]. As for the tests performed with the numerical-relativity values of $M_{\mathrm{b,torus}}$, these distributions are peaked around $\sim 0.00-0.01$ and errors higher than 2% are rare. We stress once more that large portions of the parameter space of BH-NS binaries are currently unexplored, thus preventing us from testing our approach thoroughly.

IV. RESULTS

We now review the main results obtained by systematically exploring the space of parameters of BH-NS systems using the model described so far. More specifically, we vary:

- the initial spin parameter of the BH, a_{i}, reaching a maximum value of 0.99;

- the binary mass ratio, Q, between 2 and 10;

- the NS mass, between $1.2M_{\odot}$ and $2.0M_{\odot}$, compatibly with the measurement reported in [81];

- the NS compactness. In particular, we use the WFF1 EOS [82] and the PS EOS [83] as representatives of the softest and stiffest possible EOS, yielding the most and least compact NSs, respectively. Thus, for a given NS mass we consider the compactness of a NS governed by the WFF1 EOS and the one of a NS described by the PS EOS. We also quote results for the APR2

TABLE IV. Tests against numerical-relativity results. The first six columns are organized as in Tables I and II. The last four columns show the relative error on the BH remnant gravitational mass in units of the system initial mass, $\overline{M}_{\mathrm{f}}$, on its irreducible mass in units of the system initial mass, $\overline{M}_{\mathrm{irr,f}}$, and on its $l = 2$, $m = 2$, $n = 0$ quasi-normal mode frequency, f_{220}^{QNM}, and damping time, $\tau_{220}^{\mathrm{QNM}}$.

	Ref.	EOS	C	Q	a_{i}	$\epsilon(\overline{M}_{\mathrm{f}})$	$\epsilon(\overline{M}_{\mathrm{irr,f}})$	$\epsilon(f_{220}^{\mathrm{QNM}})$	$\epsilon(\tau_{220}^{\mathrm{QNM}})$
5	[48]	$\Gamma = 2$	0.145	2	0	0.00	0.01	0.03	0.02
6	[48]	$\Gamma = 2$	0.145	3	0	0.00	0.00	0.02	0.01
7	[48]	$\Gamma = 2$	0.145	4	0	0.00	0.00	0.00	0.00
8	[48]	$\Gamma = 2$	0.145	5	0	0.00	0.00	0.01	0.00
9	[48]	$\Gamma = 2$	0.160	2	0	0.00	0.01	0.02	0.01
10	[48]	$\Gamma = 2$	0.160	3	0	0.00	0.01	0.02	0.00
11	[48]	$\Gamma = 2$	0.178	2	0	0.00	0.01	0.01	0.00
12	[48]	$\Gamma = 2$	0.178	3	0	0.01	0.01	0.01	0.01
20	[45]	2H-135	0.131	2	0	0.00	0.00	0.01	0.00
21	[45]	H-135	0.162	2	0	0.00	0.00	0.01	0.00
22	[45]	HB-135	0.172	2	0	0.00	0.01	0.01	0.00
23	[45]	HBs-135	0.172	2	0	0.00	0.01	0.01	0.00
24	[45]	HBss-135	0.174	2	0	0.00	0.01	0.01	0.00
25	[45]	B-135	0.182	2	0	0.01	0.00	0.01	0.01
26	[45]	Bs-135	0.185	2	0	0.01	0.00	0.00	0.01
27	[45]	Bss-135	0.194	2	0	0.01	0.00	0.00	0.02
28	[45]	2H-135	0.131	3	0	0.00	0.00	0.00	0.00
29	[45]	H-135	0.162	3	0	0.01	0.01	0.02	0.00
30	[45]	HB-135	0.172	3	0	0.01	0.01	0.02	0.00
31	[45]	B-135	0.182	3	0	0.01	0.01	0.01	0.01
32	[45]	2H-12	0.118	2	0	0.00	0.00	0.00	0.00
33	[45]	H-12	0.145	2	0	0.00	0.00	0.01	0.01
34	[45]	HB-12	0.153	2	0	0.00	0.00	0.01	0.00
35	[45]	B-12	0.161	2	0	0.00	0.00	0.01	0.00
36	[45]	HB-12	0.153	3	0	0.00	0.01	0.01	0.00
37	[45]	B-12	0.161	3	0	0.01	0.01	0.02	0.00

TABLE V. Same as Table IV.

|	Ref.	EOS	C	Q	a_{i}	$\epsilon(\overline{M}_{\mathrm{f}})$	$\epsilon(\overline{M}_{\mathrm{irr,f}})$	$\epsilon(f_{220}^{\mathrm{QNM}})$	$\epsilon(\tau_{220}^{\mathrm{QNM}})$
38	[44]	2H-135	0.131	2	0.75	0.01	0.02	0.04	0.04
39	[44]	1.5H-135	0.146	2	0.75	0.00	0.01	0.00	0.00
40	[44]	H-135	0.162	2	0.75	0.00	0.00	0.02	0.03
41	[44]	HB-135	0.172	2	0.75	0.00	0.01	0.02	0.03
42	[44]	B-135	0.182	2	0.75	0.00	0.01	0.02	0.03
43	[44]	2H-135	0.131	2	0.5	0.00	0.00	0.01	0.01
44	[44]	1.5H-135	0.146	2	0.5	0.00	0.00	0.01	0.01
45	[44]	H-135	0.162	2	0.5	0.00	0.00	0.00	0.00
46	[44]	HB-135	0.172	2	0.5	0.00	0.00	0.01	0.01
47	[44]	B-135	0.182	2	0.5	0.00	0.01	0.01	0.01
48	[44]	2H-135	0.131	2	−0.5	0.00	0.00	0.01	0.01
49	[44]	H-135	0.162	2	−0.5	0.00	0.00	0.01	0.00
50	[44]	HB-135	0.172	2	−0.5	0.00	0.00	0.00	0.00
51	[44]	B-135	0.182	2	−0.5	0.00	0.00	0.01	0.01
52	[44]	2H-135	0.131	3	0.75	0.00	0.01	0.01	0.00
53	[44]	1.5H-135	0.146	3	0.75	0.00	0.00	0.00	0.00
54	[44]	H-135	0.162	3	0.75	0.00	0.00	0.01	0.02
55	[44]	HB-135	0.172	3	0.75	0.00	0.01	0.02	0.01
56	[44]	B-135	0.182	3	0.75	0.01	0.00	0.01	0.02
57	[44]	2H-135	0.131	3	0.5	0.00	0.00	0.00	0.00
58	[44]	1.5H-135	0.146	3	0.5	0.00	0.00	0.00	0.00
59	[44]	H-135	0.162	3	0.5	0.00	0.01	0.01	0.00
60	[44]	HB-135	0.172	3	0.5	0.01	0.01	0.01	0.00
61	[44]	B-135	0.182	3	0.5	0.01	0.01	0.02	0.00
62	[44]	HB-135	0.172	3	−0.5	0.00	0.00	0.01	0.00
63	[44]	2H-135	0.131	4	0.75	0.00	0.01	0.01	0.01
64	[44]	H-135	0.162	4	0.75	0.01	0.00	0.02	0.04
65	[44]	HB-135	0.172	4	0.75	0.01	0.00	0.01	0.02
66	[44]	B-135	0.182	4	0.75	0.01	0.00	0.00	0.02
67	[44]	2H-135	0.131	4	0.5	0.00	0.00	0.01	0.01
68	[44]	H-135	0.162	4	0.5	0.01	0.01	0.01	0.01
69	[44]	HB-135	0.172	4	0.5	0.01	0.01	0.01	0.01
70	[44]	B-135	0.182	4	0.5	0.01	0.01	0.01	0.01
71	[44]	2H-135	0.131	5	0.75	0.00	0.01	0.02	0.03
72	[44]	H-135	0.162	5	0.75	0.01	0.00	0.01	0.02
73	[44]	HB-135	0.172	5	0.75	0.01	0.00	0.00	0.02
74	[44]	B-135	0.182	5	0.75	0.01	0.00	0.00	0.03
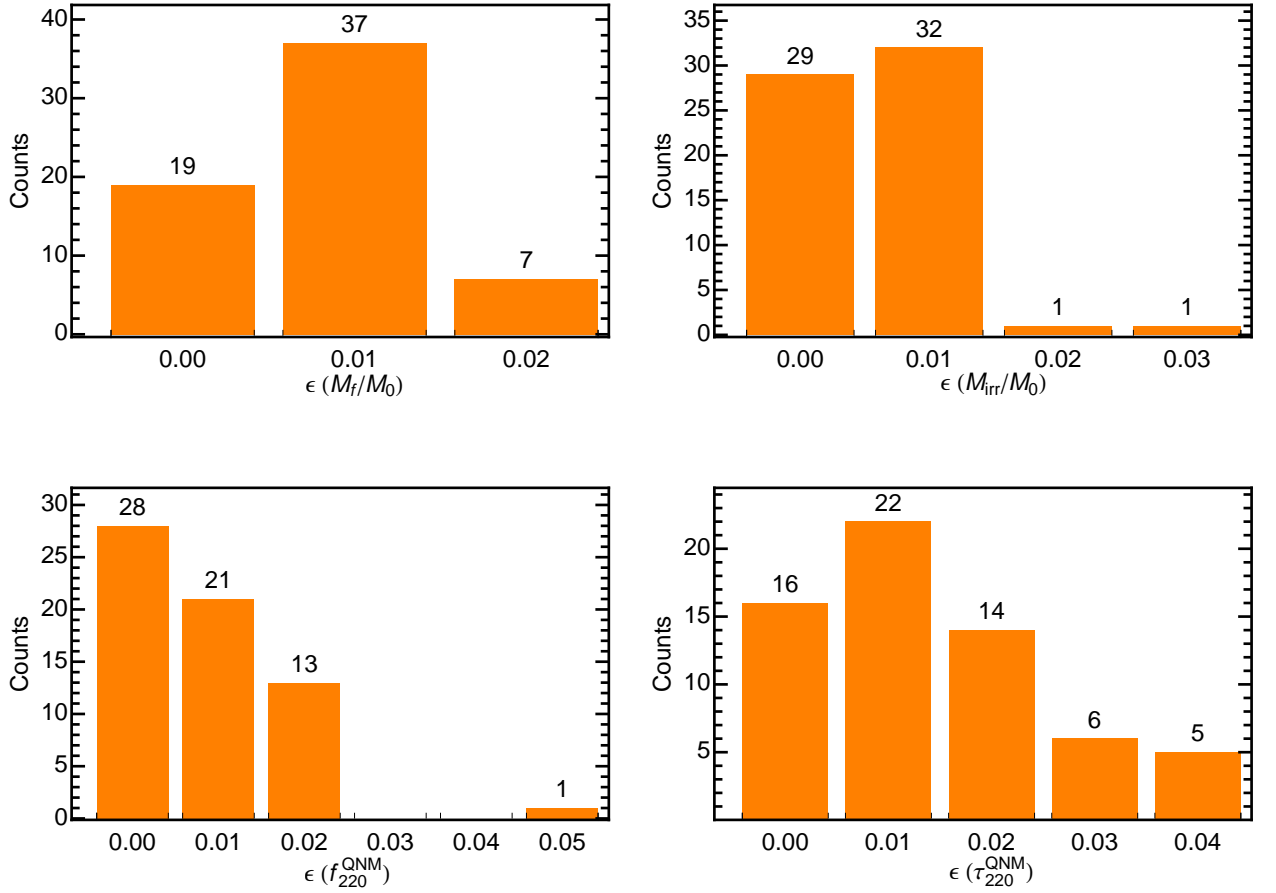
FIG. 6. Distribution of the relative errors $\epsilon(M_f/M_0)$, $\epsilon(M_{irr,f}/M_0)$, $\epsilon(f_{220}^{QNM})$, and $\epsilon(\tau_{220}^{QNM})$ obtained from Eqs. (9), (11)-(12) in combination with [1] for test-cases in Tables IV and V with $C \geq 0.14$.

EOS [84] since this is the most complete nuclear many-body study to date.

The choices regarding the EOS are discussed in detail in the Appendix.

We analyze the behaviour of a_f in the relevant space of parameters, examining its maximum possible value; we further compare the outcome of BH-NS mergers and BH-BH mergers in terms of the $l = m = 2$, $n = 0$ quasi-normal mode frequency and show that the comparison is EOS-dependent. When comparing to binary black holes, we apply the fitting formula of [75] to determine the final spin parameter of their remnants and we neglect the last term in Eq. (9) to estimate the mass of their remnants. More accurate predictions for M_f are possible for BH-BH binaries, e.g. [77]; if we were to rely on them, however, we would be comparing predictions with a different degree of accuracy, thus mixing the *physical* consequences of replacing the lower mass BH of a binary BH with a NS to effects due to the different precision underlying the compared predictions.

A. Maximum Final Spin Parameter

An important aspect to investigate when studying the final spin of the BH remnant of compact binary mergers is its maximum value. According to the cosmic censorship conjecture, the spin parameter of a BH cannot exceed unity [85]. Indirect support to the conjecture was provided by the recent numerical-relativity simulations of BH-NS mergers [44]. The extrapolation of the results of the numerical simulations to the case of an extremely spinning BH with $a_i = 1$ (merging with an irrotational NS) yielded $a_f \sim 0.98$. It was suggested that simulations with mass ratio higher than $Q = 4$ and (nearly) extremal initial BH spin should be performed in order to assess whether $a_f \lesssim 0.98(< 1)$ is a universal bound for BH-NS binary mergers or not.

Our *model* does not predict the formation of overspinning ($a_f > 1$) BHs for BH-NS binaries with an extremal initial BH spin and any symmetric mass ratio. We notice that, all else being fix, the softest the EOS, the higher the final spin parameter a_f. We thus suggest performing fully general-relativistic numerical simulations of systems with (nearly) extremal initial BH spin parameter *and* a soft NS EOS to assess the bound on $a_f < 1$ for BH-NS binary mergers.
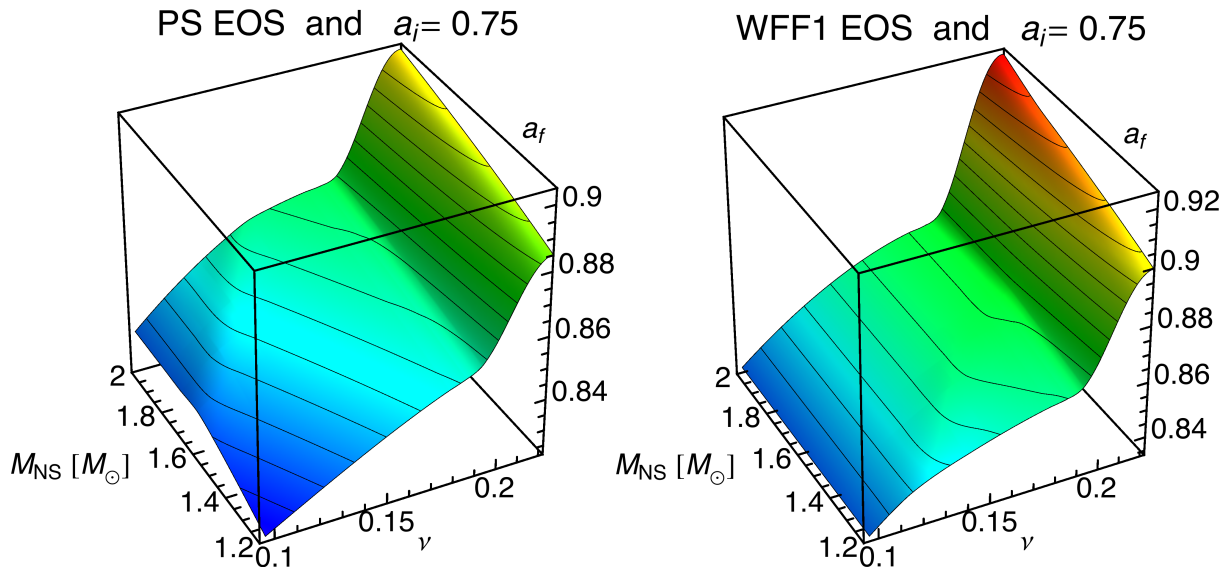
FIG. 7. (Colour online). The final spin parameter of BH-NS systems is shown as a function of the NS mass and the symmetric mass ratio; the initial spin parameter of the BH is set to 0.75. Results in the left/right panel refer to the PS/WFF1 EOS.

To determine the maximum final spin parameter, we consider our data and *extrapolate* it to $a_i = 1$. We perform the extrapolations on two different sets of data: in one case we use all our data, i.e. with a_i up to 0.99, whereas in the other we consider only $a_i \leq 0.9$. This allows us to cross-check our predictions obtained within the untested region of the parameter space $0.9 < a_i \leq 1$, thus making our conclusions more robust. The highest final spin parameters we obtain are for $Q = 10$, or $\nu \simeq 0.083$. The WFF1, PS, and APR2 EOS all yield a maximum final spin parameter $a_f = 1.00$, compatible with the $a_f \sim 0.98$ bound pinpointed in [44]. For the mass ratio $Q = 2$, on the other hand we find the maximum spin $a_f = 0.99$. Even though we previously determined that our predictions have an error $\Delta a_f \lesssim 0.02$ (see discussion in Section III), we believe it is worth mentioning that we find $\max a_f = 0.997$, an "empirical" result that is compatible with Thorne's limit of 0.998 [86].

B. Dependence of the BH Remnant on the NS EOS

The main feature that appears when comparing results for different EOSs is that final spin parameter of the BH remnant, a_f, can depend on the EOS of the NS in the mixed binary progenitor (all else being fixed). This happens because different EOSs yield different torus masses. An example of this EOS-dependence is provided in Figure 7, where binaries with $a_i = 0.75$ and two possible EOSs, the WFF1 and the PS, are considered. The EOS-dependence of a_f may be better understood by carefully examining the case of BH-BH binaries. Figure 8 shows that, given a binary with a non-spinning secondary BH and a primary BH with initial spin parameter a_i, there is a specific symmetric mass ratio that yields the maximum a_f: its value varies monotonically from 0.25 to 0 as the a_i runs from 0 to 1. More specifically, the first panel shows that for non-spinning binary BHs higher values of a_f are favoured by high symmetric mass ratios (i.e. it is "easier" to spin up a Schwarzschild BH with a mass comparable to the one of the BH itself), while this is not true in the other two panels, in which the primary BH is rotating. In the case of BH-NS systems, as one varies ν and $M_{\rm NS}$, the BH mass changes along with the mass accreting onto the BH: in the case of disruptive mergers, the latter depends on the EOS and this explains why the spin of the BH remnant depends on the EOS of the NS in the progenitor, for BH-NS disruptive mergers.

Having shown that a_f may depend on the EOS of the NS and bearing in mind that M_f may too[4], this means that information about the NS EOS is "coded" in the properties of the BH remnant. This in turn implies that the QNM spectrum of the BH remnant (1) may be affected by the EOS and (2) may deviate from the BH-BH behaviour. In Figure 9 we compare the BH remnant of BH-NS mergers to the BH remnant of BH-BH mergers. We show the difference between the QNM frequency $f_{220}^{\rm QNM}$ of the BH remnant of a BH-NS merger and of a BH-BH merger with the same secondary mass, symmetric mass ratio, and initial spin parameters. The final spin parameter and mass of the binary BHs are determined using the method of [75] and Eq. (9) without the last term, respectively. All $f_{220}^{\rm QNM}$'s are calculated using the fitting formula of [80].

Our results confirm that the mixed binaries we expect to see the most of, i.e. those with $\nu \sim 0.11$ [4], do indeed behave like binary BHs in terms of GW emission during the ringdown epoch: this is positive for template design and GW detection. In Figure 9 we show our results in the region above $\nu = 0.16$

---

[4] This is more straightforward to comprehend: NSs differing only for the EOS, differ in compactness and may thus accrete different amounts of matter in disruptive mergers with a BH, e.g. [44].
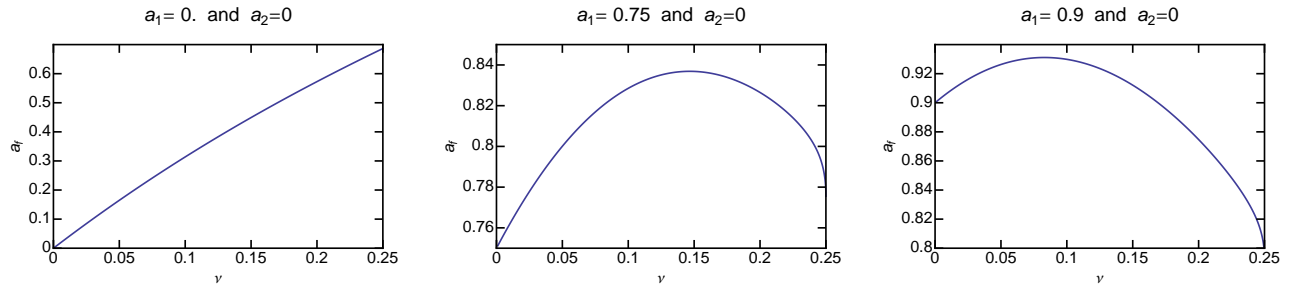
FIG. 8. (Colour online). Final spin parameter for binaries with a primary spinning BH and a secondary non-spinning BH. From left to right, the initial spin parameter of the spinning BH is set to 0, 0.75, and 0.9. The curves were obtained with the the fitting formula of [75].

for binaries with $a_{\rm i} = 0.4$ and $a_{\rm i} = 0.8$ and we contrast the PS EOS with the WFF1 EOS. We find that for $\nu \sim 0.16$ (or $Q \sim 4$) the BH remnant QNM frequency $f_{220}^{\rm QNM}$ deviates from its BH-BH binary value by $\lesssim 100$Hz for both soft and stiff EOSs, unless the initial BH spin parameter is particularly high and the NS EOS is very stiff (bottom, left panel of Figure 9). The NS thus leaves a (small) "trace" in the QNM frequency: for binaries with a BH with moderate to high spin and a symmetric mass ratio $\nu \lesssim 0.16$, one could in principle determine whether the source of a detected GW coalescence signal was a BH-BH or a BH-NS binary by separately analysing the inspiral and the ringdown epochs. The former epoch would be identical for a mixed binary and a BH binary with the same physical parameters, because tidal deformations of the NS in a mixed binary with $\nu \lesssim 0.16$ are not expected to significantly alter the inspiral epoch of the GW signal [16]. Looking at the ringdown epoch would therefore complement the idea of pinning down the presence of the NS from the inspiral. *Constraining* the NS EOS in the region of the parameter space around $\nu \sim 0.16$ by measuring $f_{220}^{\rm QNM}$ appears, instead, to be difficult.

For systems with high symmetric mass ratios, on the other hand, the difference in $f_{220}^{\rm QNM}$ may be high, suggesting the interesting prospect of constraining the NS EOS through the measurement of the properties of the BH remnant. If we now focus on the high ν region of the panels in Figure 9, we see that the deviations in $f_{220}^{\rm QNM}$ from the BH-BH case are particularly evident for $\nu \gtrsim 0.2$ and a high initial BH spin parameter. This and all other features of the bottom panels in Figure 9 may be compared to those of the panels Figure 7, showing that they are "inherited" from the behaviour of $a_{\rm f}$. At high ν's and $a_{\rm i}$'s, the difference between the $f_{220}^{\rm QNM}$ of the BH remnant of a BH-NS merger and the one of a BH-BH merger ranges from ~ 600Hz to ~ 1200Hz. The NS EOS therefore leaves an imprint on the QNM frequency of the BH remnant, although one should bear in mind that we are comparing two (extreme) EOSs that are on opposite ends in terms of stiffness, and this makes the differences between the left and the right panels of Figure 9 particularly prominent. A comparison between results for the WFF1 EOS and the APR2 EOS, which yield NSs relatively similar in terms of compactness (see Figure 11), tells us that in order to be able to properly discriminate between similar candidate nuclear EOSs, one would need to be able to perform measurements of $f_{220}^{\rm QNM}$ with a precision

the order of ~ 10Hz.

Being able to perform measurements of $f_{220}^{\rm QNM}$ for the BH remnant of BH-NS mergers requires that the QNM itself is excited during the coalescence. If this happens, $f_{220}^{\rm QNM}$ influences the value of the cutoff frequency $f_{\rm cut}$ of the the GW spectrum of the mixed binary coalescence [5]. The *extrapolation* of the results of the numerical-relativity simulations reported in [44] shows, in particular, that $f_{\rm cut} \simeq f_{220}^{\rm QNM}$ for $C \gtrsim 0.18$ in mixed binaries with $\nu \simeq 0.139$ (or $Q = 5$) and $a_{\rm i} = 0.75$, or for $C \gtrsim 0.19$ in binaries when $a_{\rm i} = 0$ and $\nu \simeq 0.22$ ($Q = 2$) or $\nu \simeq 0.1875$ ($Q = 3$) and $a_{\rm i} = 0.5$. The higher $a_{\rm i}$, the higher the lower bound on C that allows for $f_{\rm cut} \simeq f_{220}^{\rm QNM}$ to happen at a given mass ratio; on the other hand, the greater the mass of the BH at a given $a_{\rm i}$ and C, the closer $f_{\rm cut}$ will be to $f_{220}^{\rm QNM}$. The ~ 0.19 threshold on the NS compactness encountered above corresponds to $M_{\rm NS} \gtrsim 1.33 M_\odot$ for the WFF1 EOS, to $M_{\rm NS} \gtrsim 1.48 M_\odot$ for the APR2 EOS, and to $M_{\rm NS} \gtrsim 1.93 M_\odot$ for the PS EOS. We thus see that there is the virtual possibility of constraining the NS EOS with the measurement of the gravitational radiation emitted by those binaries for which $f_{\rm cut} \simeq f_{220}^{\rm QNM}$. This scenario, as said, concerns NSs with high compactnesses and would thus provide constraints for *soft* EOSs. We note that the observation of tidal effects in the phase of the gravitational radiation emitted during the inspiral [16, 87] and in the cutoff frequency when $f_{\rm cut} < f_{220}^{\rm QNM}$ [14, 44] favours placing constraints on stiff EOSs, so that measurements in $f_{\rm cut} \sim f_{220}^{\rm QNM}$ scenarios would be complementary.

V. CONCLUSIONS AND REMARKS

In this paper we presented a model for predicting the final spin parameter, $a_{\rm f}$, and mass, $M_{\rm f}$, of the BH remnant BH-NS coalescing binaries in quasi-circular orbits and with initial BH spin of arbitrary magnitude and parallel to the orbital angular momentum, arbitrary mass ratio, and arbitrary NS mass and cold, barotropic equation of state. The parameter space just outlined could in principle be investigated entirely within

---

[5] See [44] for explanations on what determines $f_{\rm cut}$ and for examples of gravitational waveform spectra.
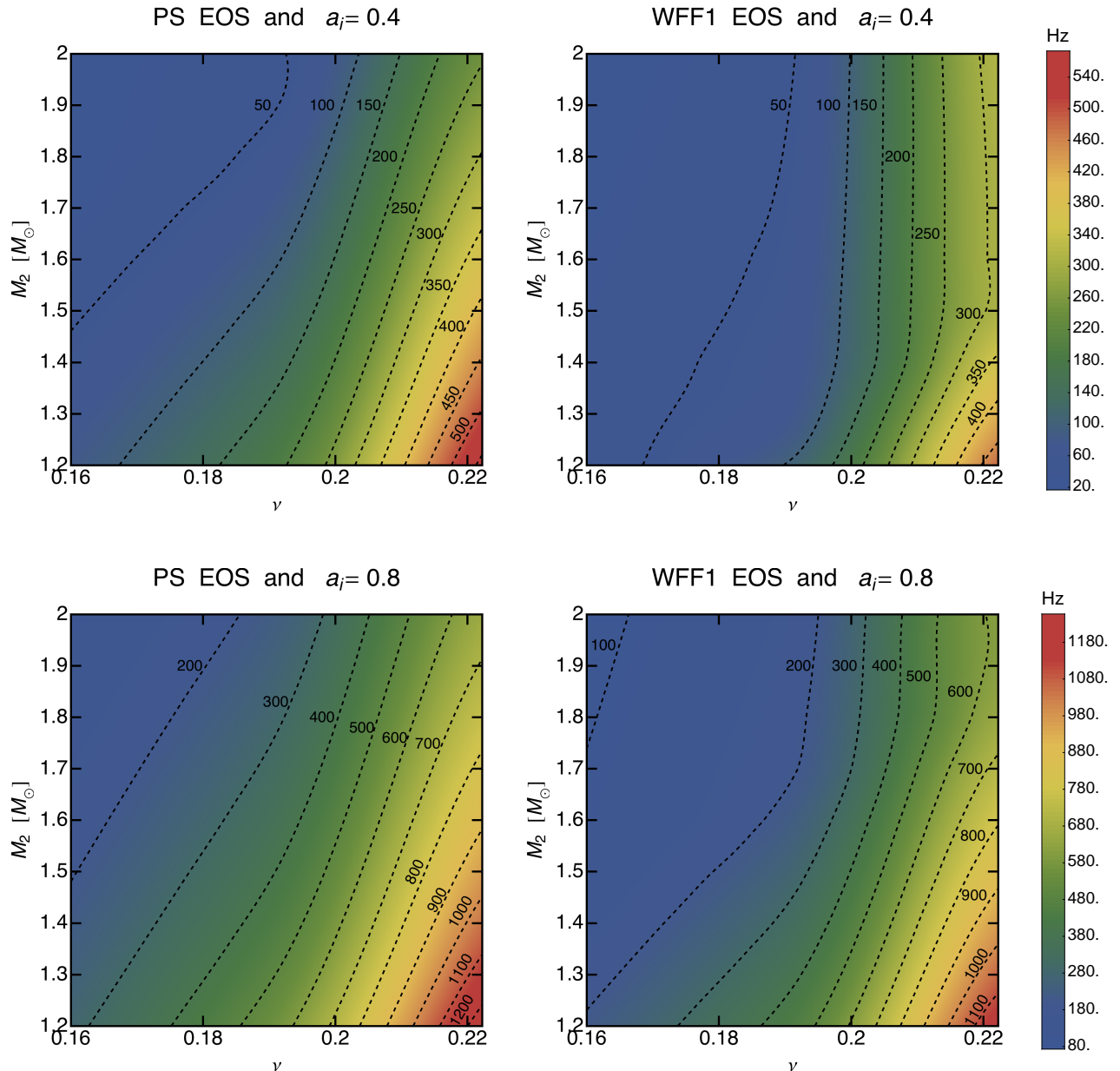
FIG. 9. (Colour online). Difference, in Hz, between the $l = m = 2$, $n = 0$ quasi-normal mode frequency, f_{220}^{QNM}, of the BH remnant of a BH-NS merger and of a BH-BH merger with the same secondary mass M_2, symmetric mass ratio ν, and initial spin parameters. The NS and secondary BH initial spin is always set to zero. The primary BH initial spin parameter is 0.4 and 0.8 in the top and bottom panels, respectively.

numerical-relativity; in practice, however, the process would be very time and resource consuming, because simulations are still very expensive in terms of computational costs.

Our starting point was the phenomenological model of Buonanno, Kidder, and Lehner for the final spin of binary BH mergers [66], which we modified to account for (1) energy loss via gravitational wave emission during the inspiral and (2) for the possible formation of an accretion torus in the case of disruptive mergers. We tested our model by comparing its predictions to the recent numerical-relativity simulation results available in the literature. We were able to achieve good agreement down to a mass ratio of $M_{\mathrm{BH}}/M_{\mathrm{NS}} = 2$, albeit in-

troducing an additional ingredient in the formulation of the model for $2 < M_{\mathrm{BH}}/M_{\mathrm{NS}} < 3$ which is currently poorly constrained. We obtained an absolute error on a_{f} of 0.02, which is compatible with the one of the BKL approach [66, 75]. For the final gravitational and irreducible (normalized) masses of the BH remnant, M_{f} and $M_{\mathrm{irr,f}}$, we found a relative error of 1%. These errors then propagate in the calculation of the $l = m = 2$, $n = 0$ quasi-normal mode frequency f_{220}^{QNM} and damping time $\tau_{220}^{\mathrm{QNM}}$ of the remnant BH and yield maximum relative errors of 4%. These relative errors are, however, safely $\leq 2\%$ in the vast majority of test-cases. Combining this method with input for the torus remnant mass from the two-

parameter model, fitted to existing numerical results, recently reported by Foucart in [1], the error $\Delta a_{\rm f} \simeq 0.02$ is preserved and so is the behaviour of the relative errors on $M_{\rm f}$, $M_{\rm irr,f}$, $f_{220}^{\rm QNM}$, and $\tau_{220}^{\rm QNM}$ (see Figures 4 and 6).

The tests we performed against the available numerical-relativity results were successful, especially considering the limitations of our simple approach. This implies that the outcome of the complicated merger dynamics of BH-NS binaries may be understood in fairly simple terms, at least when the BH initial spin and orbital angular momentum directions are parallel and the inspiral orbit is quasi-circular. Eqs. (9), (11)-(12) presented here along with the fit of Foucart to the torus remnant mass [1] constitute an easy-to-use *analytical model* that describes the remnant of BH-NS mergers. Notwithstanding the good performance of the model in the tests, its predictions should be taken with "a grain of salt", as large portions of the parameter space of BH-NS binaries are currently unexplored, hampering a thorough test of our approach.

The approach presented and tested in the first part of this work was then employed to span the space of parameters consisting of the binary (symmetric) mass ratio, the BH initial spin, the NS mass, and the NS equation of state. This enabled us to gain a sense of the behaviour of the properties of the BH remnant in this four-fold space of parameters and to pinpoint some interesting aspects which, we believe, deserve being verified and studied in conclusive, quantitative terms with the tools of numerical-relativity. The following is a summary of our main results.

- We obtained a maximum final spin parameter equal to 1.00 for the WFF1, APR2, and PS nuclear equations of state, when using the mass ratio $M_{\rm BH}/M_{\rm NS} = 10$. $M_{\rm BH}/M_{\rm NS} = 2$ yields instead a maximum final spin parameter of 0.99. Given their absolute error of 0.02, these predictions are compatible with the 0.98 maximum found in [44] and provide indirect support to the cosmic censorship conjecture [85].

- We discussed the dependence of $a_{\rm f}$ and $M_{\rm f}$ on the NS EOS, claiming that the EOS may leave an imprint on the BH remnant. The quasi-normal mode frequency $f_{220}^{\rm QNM}$ of the BH remnant, which depends on $a_{\rm f}$ and $M_{\rm f}$ alone, could thus be used to constrain the NS EOS (Figure 9). Deviations from the BH-BH values of $f_{220}^{\rm QNM}$ for symmetric mass ratios $\gtrsim 0.2$, with maximum deviations between ~ 600Hz and ~ 1200Hz. The excitation of the QNM oscillations does not occur for all mixed binary mergers, but it is likely to appear in the spectrum of the emitted gravitational radiation in the form of a cutoff frequency $f_{\rm cut} \simeq f_{220}^{\rm QNM}$ for systems with fairly compact NSs, i.e. for soft EOSs [44]. The possibility of constraining the EOS by measuring $f_{\rm cut} \simeq f_{220}^{\rm QNM}$ seems therefore complementary to other ideas for posing EOS constraints by means of GW detection, in that these favour constraints on stiff EOSs [14, 16, 44, 87]. High-frequency gravitational waves from coalescing binaries may thus turn out to be, once more, very promising in terms of the NS EOS [88].

Future applications of the approach presented in this paper may be to exploit the predicted values of $a_{\rm f}$ and $M_{\rm f}$ to (1) provide the QNM frequencies to be used in the construction of hybrid waveforms for BH-NS systems [17, 44], (2) to develop phenomenological waveforms for BH-NS systems, (3) to study time-frequency characteristics of the emitted radiation [53], and (4) to build backgrounds for perturbative approaches to the study of the post-merger epoch.

In concluding this work, we would like to stimulate the BH-NS numerical-relativity community to continue investigating different parameter configurations, as this would allow us to better constrain the current version of our model (see the discussion following Eq. (11)). Investigations on more generic initial spin configurations would also be helpful [43], as they would allow us to look into extending our approach.

Appendix A: Equations of State

NSs are the most compact objects known, lacking an event horizon. The densities in the interior of these stars are expected to exceed the equilibrium density of nuclear matter ($\rho_s \simeq 2.7 \cdot 10^{14}$ g/cm^{-3}), so their macroscopic properties, e.g. mass and radius, and the internal composition of their cores depend on the nature of strong interactions in dense matter and reflect (different aspects of) the dense matter EOS. Our knowledge about the behaviour of matter at such exceptionally high densities, however, is still currently limited. As far as the composition is concerned, for example, several dense matter models predict that — in addition to nucleons, electrons, and muons — exotica in the form of hyperons, a Bose condensate of mesons, or deconfined quark matter eventually appear at supra-nuclear densities [89].

An intense investigation to determine the EOS of dense matter was performed throughout the years [89–91]. The recent measurement of a NS with mass $M_{\rm NS} = (1.97 \pm 0.04)M_\odot$ ruled out several equations of state proposed over time [81]. NS equilibrium sequences for EOSs[6] compatible with such measurement are shown in the radius-mass plane in Figure 10. In order to assess the impact of the EOS on the BH remnant of BH-NS mergers, we pick the two EOSs that yield the smallest and the largest NS radii for any given NS mass between $\sim 1M_\odot$ and $\sim 2.1M_\odot$. We dub these two EOSs WFF1 and PS, respectively, because of their NS core description [82, 83]. The NS equilibrium sequences they

---

[6] We do not consider strange quark matter equations of state.
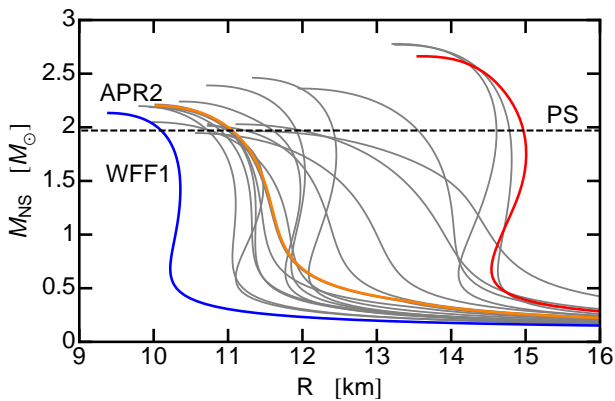
FIG. 10. (Colour online). NS equilibrium sequences in the radius-mass plane for several equations of state. The sequences shown are compatible with the recent measurement $M_{NS} = (1.97 \pm 0.04)M_\odot$ (horizontal, dashed line). Results for the WFF1/PS EOS, which yields the most/least compact NSs, are shown in blue/red. The APR2 sequence is shown in orange, while sequences obtained with other equations of state are shown with thinner, continuous gray lines.
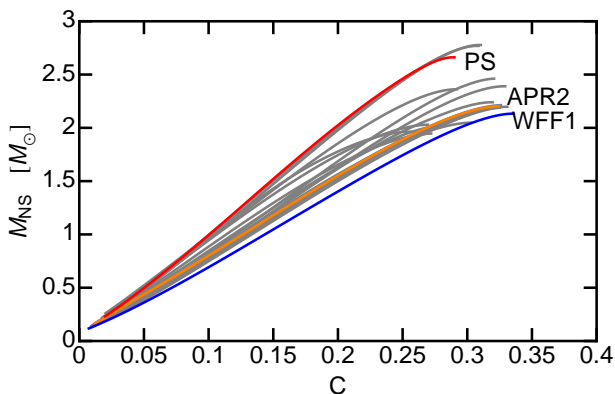

FIG. 11. (Colour online). Same as Figure 10, but in the compactness-mass plane.

yield are shown in blue and red in Figure 10. As is obvious from the graph, the WFF1 and the PS EOS bracket all other equations of state in the relevant NS mass range[7] $1.0 \lesssim M_{NS}/M_\odot \lesssim 2.1$. The sequences of Figure 10 are displayed in the compactness-mass plane in Figure 11.

For both the WFF1 and the PS EOS, we use the same description of matter in the outer layers of the NS:

- for densities in the interval starting at the neutron drip density $4 \cdot 10^{11}$ g/cm^3 and ending at $2 \cdot 10^{14}$ g/cm^3, the Pethick-Ravenhall-Lorenz (PRL) EOS [93] is used;

- for the crust layer in the density interval $(10^7 - 4 \cdot 10^{11})$ g/cm^3, the Baym-Pethick-Sutherland (BPS) EOS [94] is adopted;

- and, finally, for densities lower than 10^7 g/cm^3 the BPS EOS is extrapolated.

The two EOSs differ at densities above $2 \cdot 10^{14}$ g/cm^3: for the NS core we use what are strictly speaking the WFF1 EOS of [82] and the "liquid" version of the PS EOS of [83]. The WFF1 EOS for dense nuclear matter is based on a many-body Hamiltonian built with the Argonne v_{14} two-nucleon potential and the Urbana VII three-nucleon potential; calculations are performed with a variational method. The PS EOS, instead, considers neutron-only matter with π^0 condensates; the π^0 relativistic field is not treated explicitly but is instead replaced by an equivalent two-body potential; calculations are performed using a constrained variational method. Both WFF1 and PS are dated and have been superseded by more modern models and calculation techniques; however, they serve our purpose of considering extremely compact and extremely large NSs, respectively, to explore the space of parameters of BH-NS binaries.

In addition to the WFF1 and PS cases, we also discuss results obtained for the APR2 EOS [84], which is used as it represents the most complete nuclear many-body study to date and special-relativistic corrections were progressively incorporated in it. APR2 is based on the Argonne v_{18} two-nucleon potential, the Urbana IX three-nucleon potential, and the δv_b boost; it is supported by current astrophysical [95] and nuclear physics constraints [96].

[1] F. Foucart, ArXiv e-prints , 1207.6304 (2012).
[2] M. Shibata and K. Taniguchi, Living Reviews in Relativity **14** (2011).
[3] V. Kalogera, K. Belczynski, C. Kim, R. O'Shaughnessy, and B. Willems, Physics Reports **442**, 75 (2007).
[4] K. Belczynski, R. E. Taam, V. Kalogera, F. Rasio, and T. Bulik, Astrophys. J. **662**, 504 (2007).
[5] K. Belczynski, R. E. Taam, E. Rantsiou, and M. van der Sluys, Astrophys. J. **682**, 474 (2008).

[6] R. O'Shaughnessy, C. Kim, V. Kalogera, and K. Belczynski, Astrophys. J. **672**, 479 (2008).
[7] J. Abadie, B. P. Abbott, R. Abbott, M. Abernathy, T. Accadia, F. Acernese, C. Adams, R. Adhikari, P. Ajith, B. Allen, and et al., Classical Quantum Gravity **27**, 173001 (2010).
[8] LIGO: Laser Interferometer Gravitational Wave Observatory – http://www.ligo.caltech.edu/.
[9] Virgo – http://www.virgo.infn.it/.
[10] KAGRA: Kamioka Gravitational wave detector – http://gwcenter.icrr.u-tokyo.ac.jp/en/.
[11] M. Punturo *et al.*, Classical Quantum Gravity **27**, 084007 (2010).
[12] E. Nakar, Phys. Rep. **442**, 166 (2007).
[13] E. Berger, Nature **55**, 1 (2011).
[14] M. Vallisneri, Phys. Rev. Lett. **84**, 3519 (2000).

[7] The theoretical minimum mass for a proto-neutron star is $1.1M_\odot - 1.2M_\odot$ [92].

[15] V. Ferrari, L. Gualtieri, and F. Pannarale, Phys. Rev. D **81**, 064026 (2010).

[16] F. Pannarale, L. Rezzolla, F. Ohme, and J. S. Read, Phys. Rev. D **84**, 104017 (2011).

[17] B. D. Lackey, K. Kyutoku, M. Shibata, P. R. Brady, and J. L. Friedman, Phys. Rev. D **85**, 044061 (2012).

[18] J. M. Lattimer and D. N. Schramm, Astrophysical Journal, Letters **192**, L145 (1974).

[19] K. Taniguchi, T. W. Baumgarte, J. A. Faber, and S. L. Shapiro, Phys. Rev. D **72**, 044008 (2005).

[20] P. Grandclément, Phys. Rev. D **74**, 124002 (2006).

[21] J. A. Faber, T. W. Baumgarte, S. L. Shapiro, and K. Taniguchi, Astrophys. J. **641**, L93 (2006).

[22] J. A. Faber, T. W. Baumgarte, S. L. Shapiro, K. Taniguchi, and F. A. Rasio, Phys. Rev. D **73**, 024012 (2006).

[23] A. A. Tsokaros and K. b. o. Uryū, Phys. Rev. D **75**, 044026 (2007).

[24] K. Taniguchi, T. W. Baumgarte, J. A. Faber, and S. L. Shapiro, Phys. Rev. D **75**, 084005 (2007).

[25] K. Taniguchi, T. W. Baumgarte, J. A. Faber, and S. L. Shapiro, Phys. Rev. D **77**, 044003 (2008).

[26] H.-T. Janka, T. Eberl, M. Ruffert, and C. L. Fryer, Astrophys. J. **527**, L39 (1999).

[27] M. Ruffert and H.-T. Janka, Astron. Astrophys. **344**, 573 (1999).

[28] W. Kluzniak and W. H. Lee, Astrophysical Letters Communications **38**, 205 (1999).

[29] S. Rosswog, Astrophys. J. **634**, 1202 (2005).

[30] F. Löffler, L. Rezzolla, and M. Ansorg, Phys. Rev. D **74**, 104018 (2006).

[31] C. F. Sopuerta, U. Sperhake, and P. Laguna, Classical Quantum Gravity **23**, S579 (2006).

[32] M. Shibata and K. Uryu, Phys. Rev. D **74**, 121503 (R) (2006).

[33] M. Shibata and K. Ury, Classical Quantum Gravity **24**, S125 (2007).

[34] Z. B. Etienne, J. A. Faber, Y. T. Liu, S. L. Shapiro, K. Taniguchi, and T. W. Baumgarte, Phys. Rev. D **77**, 084002 (2008).

[35] M. Shibata and K. Taniguchi, Phys. Rev. D **77**, 084015 (2008).

[36] E. Rantsiou, S. Kobayashi, P. Laguna, and F. A. Rasio, Astrophys. J. **680**, 1326 (2008).

[37] M. D. Duez *et al.*, Phys. Rev. D **78**, 104015 (2008).

[38] Z. B. Etienne, Y. T. Liu, S. L. Shapiro, and T. W. Baumgarte, Phys. Rev. D **79**, 044024 (2009).

[39] M. Shibata, K. Kyutoku, T. Yamamoto, and K. Taniguchi, Phys. Rev. D **79**, 044030 (2009).

[40] M. D. Duez, F. Foucart, L. E. Kidder, C. D. Ott, and S. A. Teukolsky, Classical Quantum Gravity **27**, 114106 (2010).

[41] K. Kyutoku, M. Shibata, and K. Taniguchi, Phys. Rev. D **82**, 044049 (2010).

[42] S. Chawla, M. Anderson, M. Besselman, L. Lehner, S. L. Liebling, P. M. Motl, and D. Neilsen, Phys. Rev. Lett. **105**, 111101 (2010).

[43] F. Foucart, M. D. Duez, L. E. Kidder, and S. A. Teukolsky, Phys. Rev. D **83**, 024005 (2011).

[44] K. Kyutoku, O. H., M. Shibata, and K. Taniguchi, Phys. Rev. D **84**, 064018 (2011).

[45] K. Kyutoku, M. Shibata, and K. Taniguchi, Phys. Rev. D **84**, 049902 (2011).

[46] F. Foucart, M. D. Duez, L. E. Kidder, M. A. Scheel, B. Szilagyi, and S. A. Teukolsky, Phys. Rev. D **85**, 044015 (2012).

[47] Z. B. Etienne, Y. T. Liu, V. Paschalidis, and S. L. Shapiro, Phys. Rev. D **85**, 064029 (2012).

[48] M. Shibata, K. Kyutoku, T. Yamamoto, and K. Taniguchi, Phys. Rev. D **85**, 127502 (2012).

[49] M. Ruffert and H.-T. Janka, A&A **514**, A66 (2010).

[50] M. Shibata, Progress of Theoretical Physics **96**, 917 (1996).

[51] P. Wiggins and D. Lai, Astrophys. J. **532**, 530 (2000).

[52] E. Berti, S. Iyer, and C. M. Will, Phys. Rev. D **77**, 024019 (2008).

[53] C. Hanna, M. Megevand, E. Ochsner, and C. Palenzuela, Classical and Quantum Gravity **26**, 015009 (2009).

[54] V. Ferrari, L. Gualtieri, and F. Pannarale, Classical Quantum Gravity **26**, 125004 (2009).

[55] T. Damour and A. Nagar, Phys. Rev. D **81**, 084016 (2010).

[56] F. Pannarale, A. Tonita, and L. Rezzolla, Astrophys. Journ. **727**, 95 (2011).

[57] A. Buonanno and T. Damour, Phys. Rev. D **62**, 064015 (2000).

[58] T. Damour, Phys. Rev. D **64**, 124013 (2001).

[59] S. A. Hughes and R. D. Blandford, Astrophys. J. **585**, L101 (2003).

[60] A. Buonanno, Y. Chen, and T. Damour, Phys. Rev. D **74**, 104005 (2006).

[61] M. Campanelli, C. O. Lousto, and Y. Zlochower, Phys. Rev. D **73**, 061501 (2006).

[62] M. Campanelli, C. O. Lousto, and Y. Zlochower, Phys. Rev. D **74**, 041501 (2006).

[63] M. Campanelli, C. O. Lousto, and Y. Zlochower, Phys. Rev. D **74**, 084023 (2006).

[64] T. Damour and A. Nagar, Phys. Rev. D **76**, 044003 (2007).

[65] W. Tichy and P. Marronetti, Phys. Rev. D **76**, 061502 (2007).

[66] A. Buonanno, L. E. Kidder, and L. Lehner, Phys. Rev. D **77**, 026004 (2008).

[67] L. Rezzolla, E. N. Dorband, C. Reisswig, P. Diener, D. Pollney, E. Schnetter, and B. Szilágyi, Astrophys. J. **679**, 1422 (2008).

[68] L. Boyle, M. Kesden, and S. Nissanke, Phys. Rev. Lett. **100**, 151101 (2008).

[69] M. Kesden, Phys. Rev. D **78**, 084030 (2008).

[70] P. Marronetti, W. Tichy, B. Bruegmann, J. Gonzalez, and U. Sperhake, Phys. Rev. D **77**, 064010 (2008).

[71] L. Rezzolla, P. Diener, E. N. Dorband, D. Pollney, C. Reisswig, E. Schnetter, and J. Seiler, Astrophys. J. **674**, L29 (2008).

[72] L. Rezzolla, E. Barausse, E. N. Dorband, D. Pollney, C. Reisswig, J. Seiler, and S. Husa, Phys. Rev. D **78**, 044002 (2008).

[73] L. A. Gergely and P. L. Biermann, J. Phys. Conf. Ser. **122**, 012040 (2008).

[74] L. Rezzolla, Class. Quant. Grav. **26**, 094023 (2009).

[75] E. Barausse and L. Rezzolla, Astrophys. J. Lett. **704**, L40 (2009).

[76] M. Kesden, G. Lockhart, and E. S. Phinney, Phys. Rev. D **82**, 124045 (2010).

[77] E. Barausse, V. Morozova, and L. Rezzolla, ArXiv e-prints (2012).

[78] L. Bildsten and C. Cutler, Astrophys. J. **400**, 175 (1992).

[79] C. S. Kochanek, Astrophys. J. **398**, 234 (1992).

[80] E. Berti, V. Cardoso, and A. O. Starinets, Class. Quant. Grav. **26**, 163001 (2009).

[81] P. B. Demorest, T. Pennucci, S. M. Ransom, M. S. E. Roberts, and J. W. T. Hessels, Nature **467**, 1081 (2010).

[82] Wiringa, Fiks, and Fabrocini, Phys. Rev. C **38**, 1010 (1988).

[83] V. R. Pandharipande and R. A. Smith, Nuclear Physics A **237**, 507 (1975).

[84] A. Akmal and V. R. Pandharipande, Phys. Rev. C **56**, 2261 (1997).

[85] R. Penrose, *General Relativity: An Einstein Centenary Survey*, edited by S. Hawking and W. Israel (Cambridge University Press, Cambridge, England, 1979).

[86] K. S. Thorne, Astrophys. J. **191**, 507 (1974).

[87] T. Hinderer, B. D. Lackey, R. N. Lang, and J. S. Read, Phys.

Rev. D **81**, 123016 (2010).

[88] A. Bauswein, H.-T. Janka, K. Hebeler, and A. Schwenk, ArXiv e-prints (2012).

[89] J. M. Lattimer and M. Prakash, Phys. Rep. **442**, 109 (2007).

[90] M. Alford, Annual Review of Nuclear and Particle Science **51**, 131 (2001).

[91] J. M. Lattimer and M. Prakash, Nuclear Physics A **777**, 479 (2006).

[92] J. Goussard, P. Haensel, and J. L. Zdunik, Astron. and Astrophys. **330**, 1005 (1998).

[93] C. J. Pethick, D. G. Ravenhall, and C. P. Lorenz, Nuclear Physics A **584**, 675 (1995).

[94] G. Baym, C. Pethick, and P. Sutherland, Astrophys. J. **170**, 299 (1971).

[95] A. W. Steiner, J. M. Lattimer, and E. F. Brown, Astrophys. Journ. **722**, 33 (2010).

[96] K. Hebeler, J. M. Lattimer, C. J. Pethick, and A. Schwenk, Physical Review Letters **105**, 161102 (2010).